Check for updates

Advanced Functional Materials

ADVANCED FUNCTIONAL MATERIALS
www.afm-journal.de

RESEARCH ARTICLE

Pollen-Derived Paper for Sustainable Droplet Energy Harvesting

Zi Hao Guo[1,2] | Chenchen Zhou[1,3,4] | Hailu Wang[3,4] | Jian Li[3,4] | Jingyu Deng[3,4] | Yabo Huang[5] | Xiong Pu[6] | Munho Kim[2] | Namjoon Cho[3,4]

[1]State Key Laboratory of Micro-nano Engineering Science, School of Mechanical Engineering, Shanghai Jiao Tong University, Shanghai, People's Republic of China | [2]School of Electrical and Electronic Engineering, Nanyang Technological University, Singapore, Singapore | [3]School of Materials Science and Engineering, Nanyang Technological University, Singapore, Singapore | [4]Centre for Cross Economy, Nanyang Technological University, Singapore, Singapore | [5]School of Materials Science and Engineering, Zhengzhou University of Aeronautics, Zhengzhou, Henan, People's Republic of China | [6]Beijing Institute of Nanoenergy and Nanosystems, Chinese Academy of Sciences, Beijing, People's Republic of China

Correspondence: Chenchen Zhou (chenchen.zhou@sjtu.edu.cn) | Xiong Pu (puxiong@binn.cas.cn) | Munho Kim (munho.kim@ntu.edu.sg) | Namjoon Cho (njcho@ntu.edu.sg)

Received: 26 August 2026 | **Revised:** 7 October 2026 | **Accepted:** 15 October 2026

Keywords: droplet | energy harvester | pollen | triboelectric nanogenerator

ABSTRACT

Harvesting electricity from raindrops offers a promising route toward distributed self-powered electronics, but conventional devices rely predominantly on non-renewable synthetic polymers and metals. Here, we report a pollen-derived droplet energy harvester (PDEH) fabricated from abundant sunflower pollen. Defatting and mild de-esterification convert rigid pollen grains into processable microgels that form free-standing paper. Functionalization produces dielectric and conductive layers for an ultrathin multilayer device containing only 24 wt.% non-renewable solid materials. The incorporated constituents of a 3×3 cm^2 device cost approximately US$0.003, excluding processing consumables. Optimizing dielectric-layer thickness and surface fluorination yields 16.8 V from a single 37 µL tap-water droplet, with an energy-conversion efficiency of 1.26% and a maximum instantaneous power density of 63 mW m^{-2}. The approximately 70 µm-thick, 0.191 g device conforms to flat, curved, and irregular surfaces and maintains stable electrical output over 14 days of operation. A ten-unit PDEH array harvests simulated rainfall to charge a 10 µF capacitor to 2 V, subsequently powering a commercial electronic clock. These findings establish pollen-derived functional paper as a low-cost platform for droplet energy harvesting and demonstrate its potential for renewable-material-based, distributed self-powered electronic systems that combine renewable feedstocks, mechanical conformability, and energy storage for practical applications.

1 | Introduction

Since the dawn of the electrical age, electricity demand has surged in tandem with industrial growth and the electrification of everyday life. Global consumption skyrocketed from roughly 8000 TWh in 1980 to over 26 500 TWh in 2022 (continuing to grow at over 3% per year), while generation capacity expansions have repeatedly lagged behind, resulting in persistent supply shortfalls and grid reliability challenges [1, 2].

To alleviate the looming electricity shortage, many countries have historically relied heavily on thermo-mechanical power generation—notably coal, gas, and nuclear plants [3, 4]. However, these conventional approaches bring serious drawbacks.

Zi Hao Guo and Chenchen Zhou contributed equally to this work.

All rights reserved, including rights for text and data mining and training of artificial intelligence technologies or similar technologies.
© 2026 Wiley-VCH GmbH

Fossil-fuel plants emit large amounts of CO_2 and other pollutants, causing air and water pollution and exacerbating climate change. Nuclear power, while low-carbon in operation, faces unresolved issues of spent fuel disposal and the ever-present risk of nuclear accidents or leaks [5–9].

In response, nations around the world have actively promoted various clean/renewable energy sources, such as hydropower, wind power, and solar photovoltaics [10–12]. Yet, despite rapid growth in recent years, renewables still make up only a modest portion of the global electricity mix. In 2024, renewable power generation accounted for around 32% of global electricity, according to Ember's Global Electricity Review [13]. This indicates that, notwithstanding strong momentum, current clean energy penetration is still far from sufficient to satisfy the ever-rising demand and to displace fossil sources at scale. Therefore, beyond merely scaling up existing renewable capacity, it is imperative to explore new, pollution-free, and sustainable electricity generation paradigms as potential complements to the current energy portfolio, to help push the power system toward deeper decarbonization and greater stability [14–16]. While the energy contained in water, wind, and sunlight has been extensively exploited for power generation, the mechanical energy of rainfall, despite being one of the most common weather phenomena, remains largely underutilized [17]. For example, in tropical regions such as Singapore, rainfall occurs frequently, with 210 rainy days and a total precipitation of 3179.5 mm recorded in 2022 [18]. If the mechanical energy of raindrops could be effectively converted into electricity, it could help alleviate the increasing pressure on global power supply systems.

To date, only a limited number of studies have explored droplet energy harvesting as a potential energy conversion approach [17, 19]. However, most reported devices still rely heavily on synthetic polymers derived from non-renewable fossil resources and metallic components [20–22]. This dependency not only raises concerns about resource depletion, environmental degradation, and potential health risks, but also contradicts the fundamental aim of developing sustainable energy technologies.

Therefore, it is highly desirable to explore the feasibility of utilizing naturally abundant materials for droplet energy harvesting applications, through eco-friendly, sustainable, and cost-effective processing and fabrication strategies to reduce the proportion of nonrenewable resources used. Such efforts could pave the way toward scalable, green energy harvesting systems that complement existing renewable technologies.

Among various natural materials, pollen grains are abundant, low-cost, and environmentally benign, being an agricultural byproduct that can be collected in large quantities without ecological burden [23–25]. Structurally, a pollen grain consists of two mechanically distinct layers: a rigid outer exine made of sporopollenin and a soft inner intine composed of polysaccharides, mainly cellulose, hemicellulose, and pectin. The cross-linked sporopollenin network endows the exine with remarkable stiffness, elasticity, and resistance to chemical degradation [26–29]. Through a mild alkaline treatment analogous to traditional soap making, the highly esterified pectin in the intine is de-esterified into hydrophilic, ionizable pectate; together with the removal of internal cytoplasmic contents and softening of the pollen shell, this transforms the naturally hard pollen grains into soft, hydrated microgels [30]. Subsequent casting and drying of these microgels yield a free-standing, mechanically stable, and environmentally friendly "pollen paper" [31], as shown in Figure 1a,b.

In this work, we developed a pollen-derived droplet energy harvester (PDEH) capable of converting the mechanical energy of raindrops into electricity. To construct the device, raw sunflower pollen papers were selectively modified with either perfluorodecyltrichlorosilane (FDTS) or aniline, forming dielectric and conductive pollen layers, respectively. These layers were then laminated via a hot-pressing process to assemble the final PDEH structure, as schematically illustrated in Figure 1c. By incorporating pollen paper as the primary structural material, the mass fraction of non-renewable solid materials in a single 3 × 3 cm^2 PDEH was reduced to 24%. The direct material cost of the constituents incorporated into the final device was estimated to be approximately US$0.003 (see Note S1); a laboratory-scale lower-bound estimate of the additional processing consumables is provided in Table S1. After optimizing both the dielectric layer thickness and FDTS concentration, the device could generate an output voltage of 16.8 V from a single tap-water droplet (37 μL), achieving an overall energy conversion efficiency of 1.26%. To demonstrate its practical feasibility under natural conditions, we further established a PDEH array consisting of 10 units, which was directly exposed to simulated rainfall. Each individual unit delivered a power density of 63 mW m^{-2}, and the integrated array successfully charged a 10 μF capacitor to 2 V within 80 s, subsequently powering an electronic clock for 7 s. The fabricated PDEH is ultrathin (≈70 μm) and ultralight (0.191 g), exhibiting excellent flexibility and mechanical conformability. These features allow easy integration onto curved or irregular surfaces, such as building facades, raincoats, rooftops, and plant leaves (Figure 1d). Given its decent output performance, use of abundant and renewable pollen as the primary structural feedstock, and relatively low mass fraction of non-renewable solid materials, the PDEH represents a promising step toward sustainable, low-carbon, and distributed energy harvesting technologies, offering new opportunities for future eco-friendly energy generation.

2 | Results

2.1 | Functional Design of the Pollen-Derived Droplet Energy Harvester

To fabricate the pollen paper, raw sunflower bee pollen was first subjected to a defatting process to remove the pollenkitt, which is a lipid-rich sticky coating naturally present on the pollen surface. Pollen grains contain a sporopollenin-rich exine and a polysaccharide-rich intine containing cellulose, hemicellulose, and pectin. Under alkaline treatment, de-esterification of pectin within the intine converts esterified pectin into more hydrophilic pectate, promoting hydration and swelling. Together with treatment-induced softening/remodeling of the pollen shell, these changes transform rigid pollen grains into soft microgels. The obtained pollen microgel suspension was then cast into a mold, followed by controlled evaporation of water under ambient conditions to yield the final free-standing pollen paper.

16163028, 0, Downloaded from https://advanced.onlinelibrary.wiley.com/doi/10.1002/adfm.79211 by Nam-Joon Cho - Shanghai Jiaotong University , Wiley Online Library on [21/10/2026]. See the Terms and Conditions (https://onlinelibrary.wiley.com/terms-and-conditions) on Wiley Online Library for rules of use; OA articles are governed by the applicable Creative Commons License

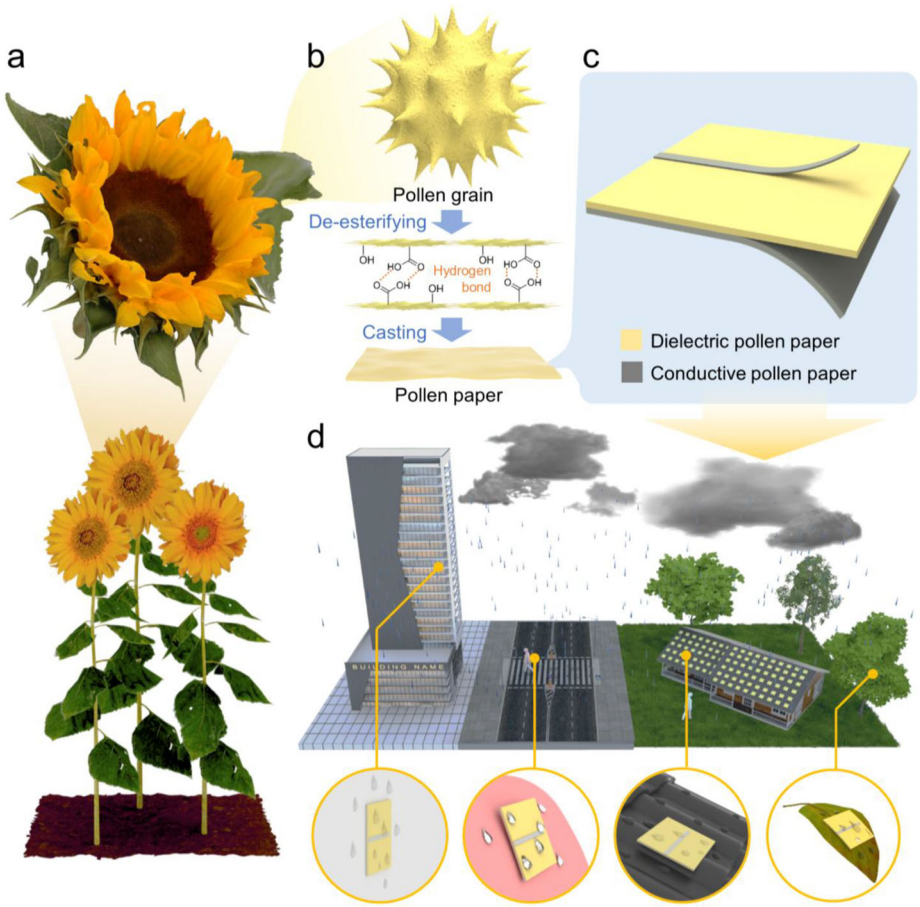


FIGURE 1 | Design and concept of the pollen-derived droplet energy harvester (PDEH). (a) Natural source of sunflower pollen and representative sunflower field, highlighting the abundant and renewable origin of the raw material. (b) Schematic illustration of the fabrication process from pollen grains to free-standing pollen paper, including defatting, de-esterification to form pollen microgels, casting, and natural drying. (c) Structural architecture of the multilayer PDEH, composed of a fluorinated dielectric pollen paper and a conductive polyaniline (PANI)-coated pollen paper, integrated via hot pressing. (d) Conceptual demonstration of the flexible and lightweight PDEH applied in diverse practical scenarios, such as building facades, rooftops, raincoats, and plant leaves, for distributed rain-energy harvesting.

However, the as-fabricated pristine pollen paper possesses abundant surface carboxyl groups, rendering it hydrophilic and exhibiting limited triboelectric performance, which is unfavorable for efficient raindrop energy collection. To overcome this limitation, fluorinated functional groups were grafted onto the pollen paper surface via hydrolysis and subsequent dehydration of perfluorodecyltrichlorosilane (FDTS). Specifically, the pollen paper was immersed in an FDTS–ethanol solution. The trace amounts of water inherently present in both the ethanol solvent and the pollen paper first induced hydrolysis of FDTS, yielding R—$Si(OH)_3$ intermediates (R represents —$(CF_2)_8$-CF_3). Under the water-deficient environment of the ethanol medium, a subsequent dehydration condensation occurred between the silanol groups (R—$Si(OH)_3$) and the surface carboxyl groups of the pollen paper, resulting in the covalent grafting of fluorine-containing chains onto the surface [32]. The introduced fluorinated groups endowed the pollen paper with hydrophobicity, preventing water permeation and swelling, while simultaneously enhancing negative charge affinity due to the high electronegativity of fluorine, thereby improving its triboelectric performance [33–35]. As shown in Figure 2a, after FDTS modification, the water contact angle increased markedly from 65.38° to 111.79°, confirming the successful hydrophobic functionalization. The chemical composition change was further verified by X-ray photoelectron spectroscopy (XPS). As shown in Figure 2c, in addition to the C 1s and O 1s peaks, a prominent F 1s peak at 686 eV appeared in the FDTS-treated sample, indicating the presence of fluorine species [36]. The high-resolution C 1s spectra (Figure 2d) revealed components corresponding to C—F_2 and C—F_3 bonds, providing further evidence of successful fluorination. Moreover, the FTIR spectra (Figure S2) displayed characteristic peaks at 1197 cm^{-1} (—CF_2—) and 1376 cm^{-1} (—CF_2—CF_3), which remained stable even after 14 days, demonstrating the durability of the fluorine grafting on the pollen paper surface [37]. In addition, as shown in Figure S3 and Figure 2e, a comparison between the SEM images of the pristine and FDTS-modified pollen papers revealed no noticeable change in surface morphology. This observation confirms that the fluorinated groups were grafted at the molecular level. Such a modification requires only a trace amount of FDTS to achieve the desired surface performance, thereby further contributing to cost reduction in the overall device fabrication. This fluorination strategy effectively enhanced the dielectric properties and charge-trapping ability of the pollen paper, laying the foundation for high-performance droplet energy harvesting in the PDEH.

16163028, 0, Downloaded from https://advanced.onlinelibrary.wiley.com/doi/10.1002/adfm.79211 by Nam-Joon Cho - Shanghai Jiaotong University , Wiley Online Library on [21/10/2026]. See the Terms and Conditions (https://onlinelibrary.wiley.com/terms-and-conditions) on Wiley Online Library for rules of use; OA articles are governed by the applicable Creative Commons License

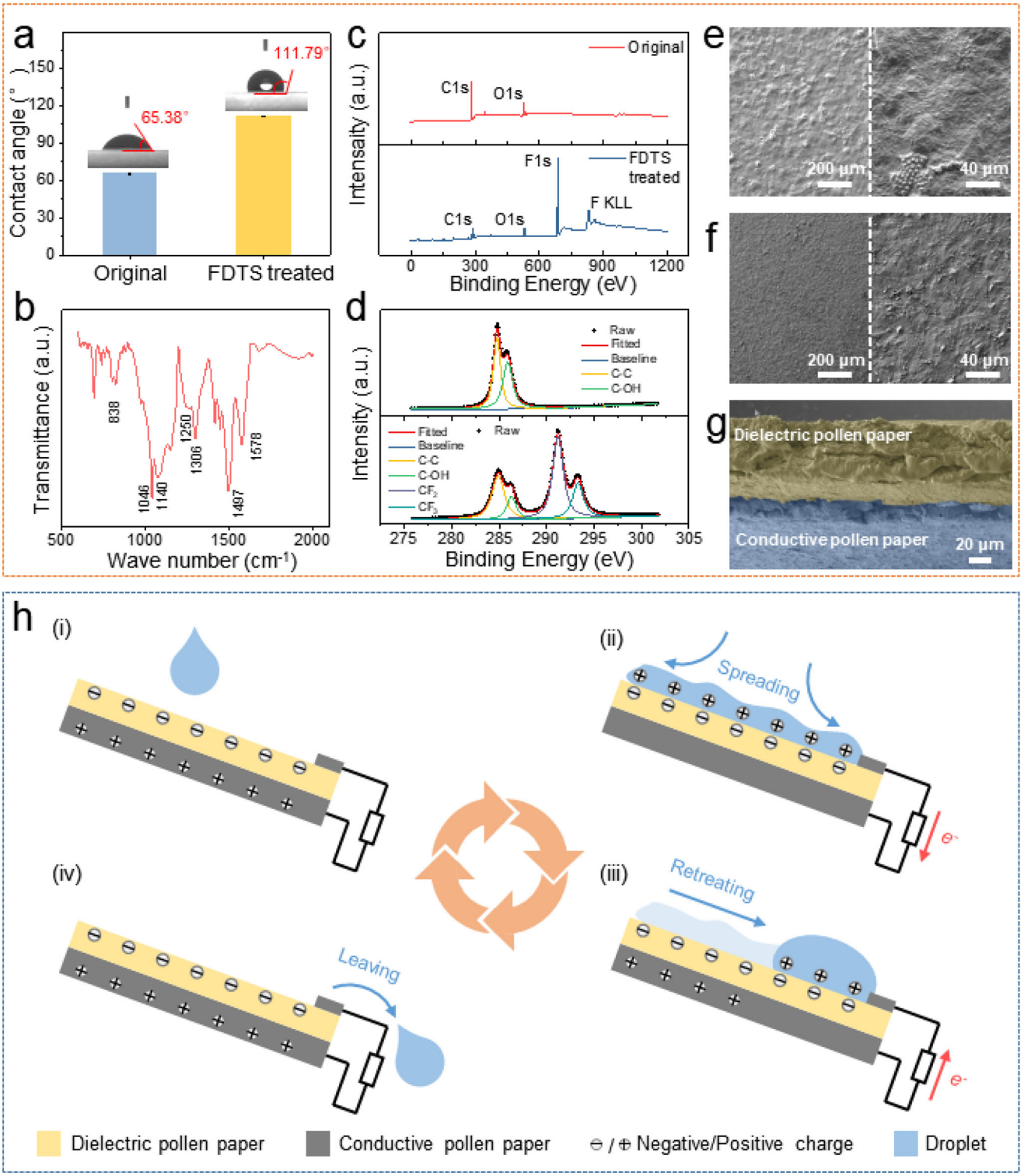


FIGURE 2 | Surface characterization and working mechanism of the pollen-derived droplet energy harvester (PDEH). (a) Static water contact angles of pristine and FDTS-modified pollen paper, demonstrating the transition from hydrophilic to hydrophobic surface after fluorination. (b) FTIR spectrum of the HCl-doped polyaniline (PANI)-coated conductive pollen paper, confirming successful in situ polymerization and protonation of aniline. (c) XPS survey spectra of pristine and FDTS-treated pollen paper, showing the emergence of the F 1s peak after surface fluorination. (d) High-resolution C 1s spectra of pristine and FDTS-modified pollen paper, revealing the formation of C—F_2 and C—F_3 bonds. (e, f) SEM images of the dielectric (FDTS-modified) and conductive (PANI-coated) pollen paper surfaces, indicating preserved morphology and formation of a continuous conductive coating. (g) Cross-sectional SEM image of the multilayer PDEH assembled by hot pressing, illustrating the compact interface between dielectric and conductive layers. (h) Schematic illustration of the working principle of the PDEH, depicting charge induction, droplet spreading and retraction, and the cyclic charge transfer process during droplet impact.

16163028, 0, Downloaded from https://advanced.onlinelibrary.wiley.com/doi/10.1002/adfm.79211 by Nam-Joon Cho - Shanghai Jiaotong University , Wiley Online Library on [21/10/2026]. See the Terms and Conditions (https://onlinelibrary.wiley.com/terms-and-conditions) on Wiley Online Library for rules of use; OA articles are governed by the applicable Creative Commons License

To impart electrical conductivity, a thin layer of HCl-doped polyaniline (PANI) was subsequently deposited onto another pollen paper surface. The successful formation of the conducting layer was confirmed by FTIR spectroscopy (Figure 2b). The characteristic absorption bands at 1578 and 1497 cm^{-1} correspond to the quinoid and benzenoid ring stretching vibrations, respectively. The band observed at 1306 cm^{-1} is attributed to π-electron delocalization induced in the polymer backbone upon protonation. In addition, the band at 1250 cm^{-1} is assigned to the C—N^+ stretching vibration associated with the polaron structure. The absorption near 1140 cm^{-1} arises from the —NH^+= vibration mode, indicating protonation of nitrogen atoms within the polymer chain. Meanwhile, the peaks at 1046 and 838 cm^{-1} correspond to C—Cl and C—H out-of-plane vibrations, respectively [38, 39]. Collectively, these spectral features, together with the SEM observations shown in Figure 2f, confirm the successful in situ polymerization of aniline on the pollen paper surface and the formation of a continuous conductive coating. The resulting conductive pollen paper exhibited a surface resistance of approximately 70 kΩ, demonstrating sufficient conductivity for its function as the electrode layer in the pollen-derived droplet energy harvester.

To assemble the complete device, a hot-pressing technique was employed to integrate the dielectric and conductive pollen papers into a single multilayer structure. As shown in the cross-sectional SEM image (Figure 2g), the two layers were tightly bonded, forming a compact interface with an overall thickness of approximately 70 μm (excluding the narrow top electrode). The optical image of the resulting device is presented in Figure S4. Owing to its small thickness, the PDEH can be easily folded or conformably attached to curved surfaces, exhibiting excellent mechanical flexibility suitable for various practical applications.

The working principle of PDEH is schematically illustrated in Figure 2h. As discussed in the previous section, a large number of fluorine groups are present on the surface of the dielectric pollen paper. Owing to the high electronegativity of fluorine, the dielectric pollen paper tends to accumulate negative charges on its surface, while an equal amount of induced positive charges appears in the underlying conductive layer through electrostatic induction (Figure 2h(i)). When a droplet impacts the device surface, it spreads rapidly across the dielectric layer and electrically bridges the top and bottom electrodes. During this contact process, a portion of the positive charges in the lower conductive layer flows through the external circuit into the droplet (Figure 2h(ii)). As the droplet retracts due to gravity and surface tension, the contact area decreases, and the transferred charges flow back to the lower electrode (Figure 2h(iii)). Once the droplet completely detaches from the surface, the system returns to its initial electrostatic state, completing one full energy generation cycle (Figure 2h(iv)).

2.2 | Performance Characterization and Optimization of the Pollen-Derived Droplet Energy Harvester

The typical time-resolved voltage waveform of the PDEH under a single droplet impact is shown in Figure 3a, clearly revealing four distinct stages of electricity generation. To gain deeper insight into the underlying mechanism, the energy conversion process can be further interpreted through an equivalent circuit model, as illustrated in Figure 3b. In this model, the entire PDEH behaves analogously to a transistor-like structure, where the droplet functions as a transient switch connecting the dielectric and conductive layers. The equivalent circuit consists of three capacitors connected in series: the capacitance of the dielectric pollen paper (C_p) and two electrical double-layer (EDL) capacitances, namely C_{EDL1} at the water/dielectric interface and C_{EDL2} at the water/conductive electrode interface. These capacitors are in series with three resistors, representing the resistance of the droplet (R_D), the conductive pollen paper (R_E), and the external load (R_L). Therefore, when a droplet connects to the top conductive pollen paper, capacitor C_P will charge C_{EDL2} till reaching the balance [40, 41]. Accordingly, the output voltage (V) of the PDEH can be expressed as the Equation S4. Based on this theoretical model, several key parameters influencing the output performance of the PDEH were systematically investigated.

Figure 3c illustrates the relationship between the dielectric pollen paper thickness (d) and the output voltage of the PDEH. A thin dielectric layer tends to cause electrical leakage, leading to energy loss and reduced charge retention. As the dielectric layer becomes thicker, its charge storage capacity increases, thereby enhancing the transferred charge ($Q_{transfer}$). However, when the thickness continues to increase, the electric field intensity between the solid interfaces (i.e., between the dielectric pollen paper and the bottom conductive layer) is gradually weakened, which in turn reduces Q_{transfer} [41, 42]. Consequently, as the dielectric pollen paper thickness increased from 25 to 100 μm, the output voltage first increased and then decreased, reaching its maximum value at 55 μm. This trend aligns well with the theoretical model, indicating the existence of an optimal dielectric thickness that balances charge storage and field strength for efficient droplet energy conversion.

We further investigated the effect of FDTS concentration during the fabrication process on the electrical performance of the PDEH. As shown in Figure 3d, the device output increased with increasing FDTS concentration and reached a saturation point around 1.0 wt.%, beyond which no significant enhancement was observed even when the concentration was further increased to 1.5 wt.%. A higher FDTS concentration facilitates the grafting of more fluorine groups onto the pollen paper surface within the same treatment duration (Figure S5). The increased fluorination leads to a higher surface charge density, thereby directly enhancing the $Q_{transfer}$ and voltage output. However, once the concentration reaches 1.0 wt.%, the available reactive sites on the pollen paper surface become nearly saturated, and further increasing the concentration contributes little additional grafting.

The output performance of the PDEH is also strongly influenced by the morphology and dynamics of droplets on the device surface. We first examined the effect of droplet volume on electrical output. As the droplet volume increased, the spreading area of the droplet also expanded, resulting in a higher amount of transferred charge ($Q_{transfer}$). However, when the droplet volume continued to increase, the enlarged spreading area led to a larger time constant (τ) and a slower discharge rate of the capacitor (C_p), thereby reducing the overall output voltage. In practice, the droplet volume during rainfall typically ranges from 0.2 to 78 μL,

16163028, 0, Downloaded from https://advanced.onlinelibrary.wiley.com/doi/10.1002/adfm.70211 by Nam-Joon Cho - Shanghai Jiaotong University , Wiley Online Library on [21/10/2026]. See the Terms and Conditions (https://onlinelibrary.wiley.com/terms-and-conditions) on Wiley Online Library for rules of use; OA articles are governed by the applicable Creative Commons License

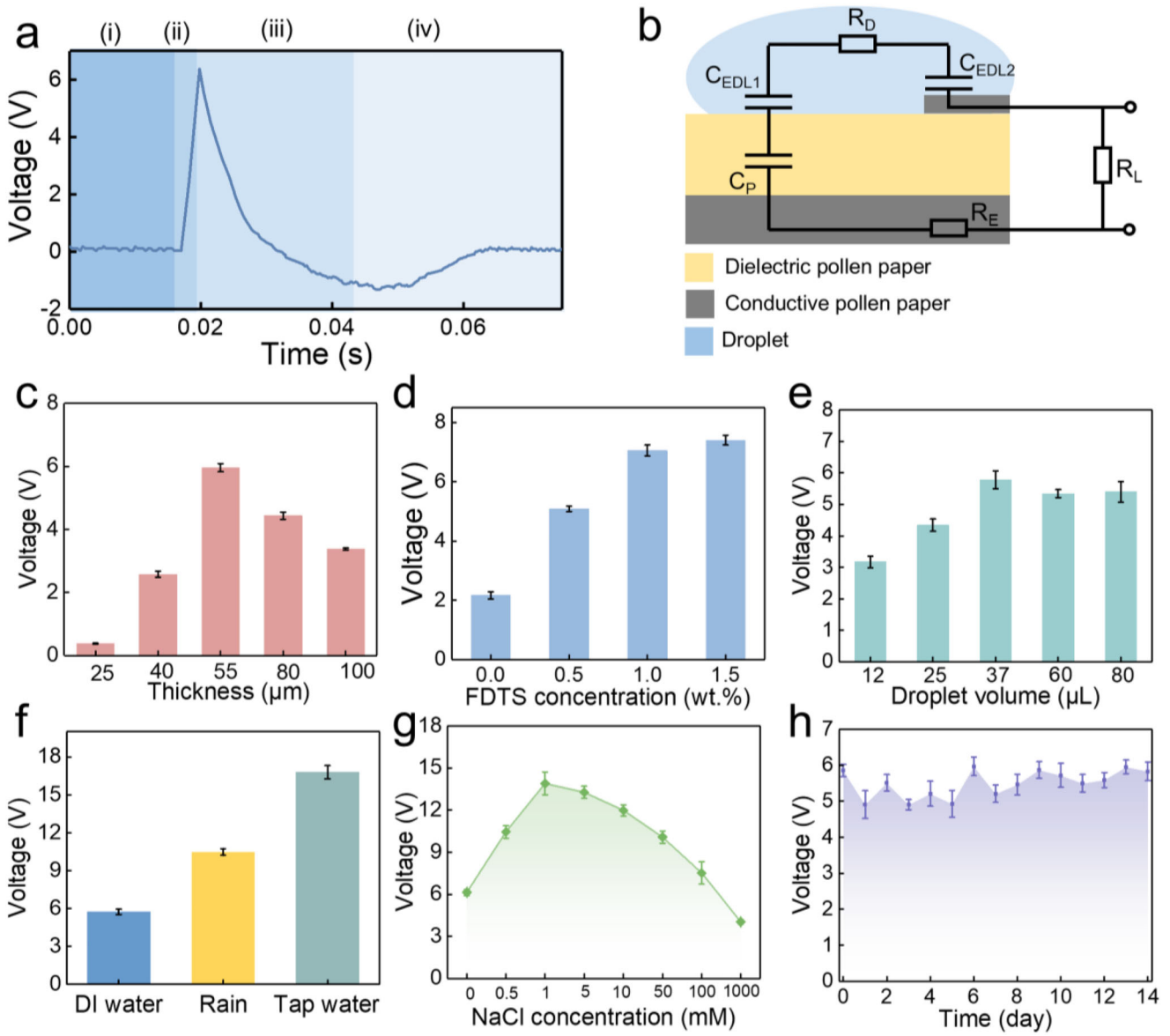


FIGURE 3 | Performance investigation and parameter optimization of the pollen-derived droplet energy harvester (PDEH). (a) Typical time-resolved output voltage waveform under a single droplet impact, showing four distinct stages (i–iv) corresponding to droplet spreading, maximum contact, retraction, and detachment, as illustrated in figure 2h. (b) Equivalent circuit model of the PDEH, describing the series combination of dielectric capacitance, electrical double-layer capacitances, and resistive elements. (c–e) Dependence of the output voltage on key structural and dynamic parameters: (c) dielectric pollen paper thickness, revealing an optimal thickness for balancing charge storage and electric field strength; (d) FDTS concentration, showing surface fluorination saturation behavior; (e) droplet volume, demonstrating a parabolic trend governed by spreading area and discharge dynamics. (f) Output performance triggered by different water types (DI water, tap water, and rainwater), highlighting the influence of liquid conductivity. (g) Voltage response as a function of NaCl concentration, exhibiting an optimal ionic concentration for maximum charge transfer. (h) Long-term durability of the PDEH, showing stable output over 14 days of repeated operation. Data in (c–h) are presented as mean ± SD of $n = 10$ repeated droplet impacts on the same PDEH device for each experimental condition.

as reported for Singapore's rainfall conditions, where an average droplet volume of approximately 24 μL corresponds to moderate rain, and about 78 μL to heavy rain [43]. Combining these data with the results in Figure 3e, it can be concluded that heavier rainfall, characterized by larger droplets, produces higher electrical outputs. In addition, we investigated the effects of droplet release height and device inclination angle on the output (Figures S6 and S7). Similarly, as the release height or inclination angle increased, the spreading area of the droplet also increased. Both parameters exhibited a parabolic dependence on output performance, with the maximum output obtained at a release height of 35 cm or an inclination angle of 30°. Furthermore, heavier rainfall is typically accompanied by a higher droplet impact frequency, which also enhances the total generated electricity. As shown in Figure S8, an increase in impact frequency results in a proportional rise in the accumulated electrical output.

Considering the variety of water sources encountered in daily environments, we also investigated the influence of water type on the electrical output of the PDEH. As shown in Figure 3f,

16163028, 0, Downloaded from https://advanced.onlinelibrary.wiley.com/doi/10.1002/adfm.79211 by Nam-Joon Cho - Shanghai Jiaotong University , Wiley Online Library on [21/10/2026]. See the Terms and Conditions (https://onlinelibrary.wiley.com/terms-and-conditions) on Wiley Online Library for rules of use; OA articles are governed by the applicable Creative Commons License

three types of water (deionized (DI) water, tap water, and rainwater) were tested. Among them, tap water produced the highest output, with a single droplet generating an output voltage of 16.8 V and an overall energy conversion efficiency of 1.26% (see Note S3). This variation can be attributed to the different conductivities of the water samples: approximately 1 μS cm^{-1} for DI water, 127 μS cm^{-1} for tap water, and 51 μS cm^{-1} for rainwater. To further verify the effect of ionic conductivity, NaCl solutions with different concentrations were tested (Figure 3g). As the NaCl concentration increased, the output voltage first increased and then decreased, reaching a maximum at 0.001 M. When the concentration rose from 0 to 0.001 M, the increased number of mobile ions in the solution facilitated stronger electrostatic induction at the PDEH surface, resulting in greater charge transfer ($Q_{transfer}$). However, when the ion concentration increased further, the solution conductivity became excessively high, which enlarged the time constant (τ) and slowed the discharge process, thereby reducing the overall output voltage.

As shown in Figure 2g, the overall thickness of the PDEH is only ~70 μm, which endows the device with excellent mechanical flexibility. It can be easily attached or conformed to surfaces with different geometries. To evaluate its adaptability, the output performance of the PDEH was tested when attached to surfaces of various shapes, including flat, curved (arc), and right-angled surfaces. As presented in Figures S9 and S10, the device continued to generate stable output in all configurations, although the absolute output varied with the droplet-impact geometry on curved and angled surfaces, confirming its functional robustness and conformability. We also subjected the PDEH to 10 000 repeated bending cycles and monitored its electrical output every 1000 cycles (Figure S13). The output showed no noticeable decrease over 10 000 bending cycles, confirming its mechanical durability under repeated deformation. These results highlight the great potential of the PDEH for integration onto irregular or flexible substrates, such as building facades, raincoats, or plant leaves, for practical rain energy harvesting applications.

Owing to the chemical stability of the grafted fluorine groups, the PDEH exhibited excellent durability during long-term operation. As shown in Figure 3h, the electrical output remained nearly unchanged after continuous testing for 14 days, demonstrating the high stability and reliability of the device under ambient conditions. In addition, the water collected after 10 000 contact cycles were analyzed by FTIR spectroscopy (Figure S11), which showed no detectable difference compared with the original water sample. Notably, no fluorine-related absorption peaks were observed, indicating that the grafted fluorine groups remained stably bound to the pollen paper surface and did not leach into the water droplets. This result confirms the environmental safety of the PDEH and demonstrates that its surface modification does not pose a risk of fluorine contamination. The water resistance was also evaluated gravimetrically: after immersion in water for 12 h, the mass increase of the FDTS-modified pollen paper is only ~2.7% (Figure S12), while that of the pristine pollen paper is ~217.1%, confirming that the fluorinated surface effectively suppresses water uptake and swelling.

2.3 | Application of the Pollen-Derived Droplet Energy Harvester

To evaluate the performance of the PDEH under rainfall conditions, a laboratory setup was constructed, as schematically illustrated in Figure 4a. The system consisted of a water reservoir, a pipe array, and a PDEH array. Collected rainwater was poured into the reservoir to generate simulated rainfall. A total of 10 PDEH units were placed beneath the falling droplets to convert the mechanical energy of raindrops into electrical energy on a scalable level. As shown in Figure 4b, each of the ten units was equipped with an individual bridge rectifier, and the rectified outputs were connected in parallel to maximize charge transfer and overall output.

Since the original output of the PDEH is alternating current (AC), rectifier circuits were employed to convert the AC output into direct current (DC), allowing the generated electricity to be subsequently stored in energy storage devices, such as capacitors or batteries (Figure 4c). The power density of a single PDEH unit was further evaluated under varying external resistive loads ranging from 10^3 to 5×10^6 Ω (Figure 4d). Upon the impact of a single rainwater droplet in an active area of 3×3 cm^2, a maximum instantaneous power density of 63 mW m^{-2} was achieved when the external load was 0.28 MΩ. Compared with representative biodegradable or cellulose-based droplet energy harvesters, the PDEH achieves a competitive power density of 63 mW m^{-2}, which is higher than those reported for the selected environmentally friendly systems summarized in Table S2. This comparison suggests that the use of pollen as a renewable structural material does not necessarily require a substantial compromise in electrical output. We note that the absolute output of the PDEH remains lower than that of state-of-the-art droplet energy generators built from fluoropolymer films and metal electrodes [17, 40], and further improvements in surface charge density and interfacial design are expected to narrow this gap. This indicates a promising application potential for practical droplet energy harvesting and related self-powered electronics.

A series of capacitors were then employed as energy storage units to evaluate the charging performance of the PDEH array. As shown in Figure 4e, PDEH arrays consisting of 10, 5, and 1 unit were able to charge a 1 μF capacitor to 2 V within 18, 27, and 45 s, respectively. Furthermore, the 10-unit PDEH array could charge capacitors of different capacitances, 1, 2.2, 4.7, and 10 μF, to 2 V within 19, 27, 48, and 79 s, respectively (Figure 4f).

The integrated PDEH array was subsequently utilized as the sole power source to operate a commercial electronic clock. As presented in Figure 4g and Movie S1, the PDEH array successfully charged a 10 μF capacitor to 2 V within approximately 80 s, and the stored electrical energy powered the clock for about 7 s. This closed-loop demonstration clearly validates the practical applicability of the PDEH for direct rain-energy harvesting and storage, showcasing its potential as a sustainable and self-powered energy system. In order to evaluate the maximum performance of this system, we further replaced the rainwater with tap water. As shown in Figure S14, when triggered by tap water, a single device generated a rectified output voltage of up to ≈13 V. In addition,

16163028, 0, Downloaded from https://advanced.onlinelibrary.wiley.com/doi/10.1002/adfm.70211 by Nam-Joon Cho - Shanghai Jiaotong University , Wiley Online Library on [21/10/2026]. See the Terms and Conditions (https://onlinelibrary.wiley.com/terms-and-conditions) on Wiley Online Library for rules of use; OA articles are governed by the applicable Creative Commons License

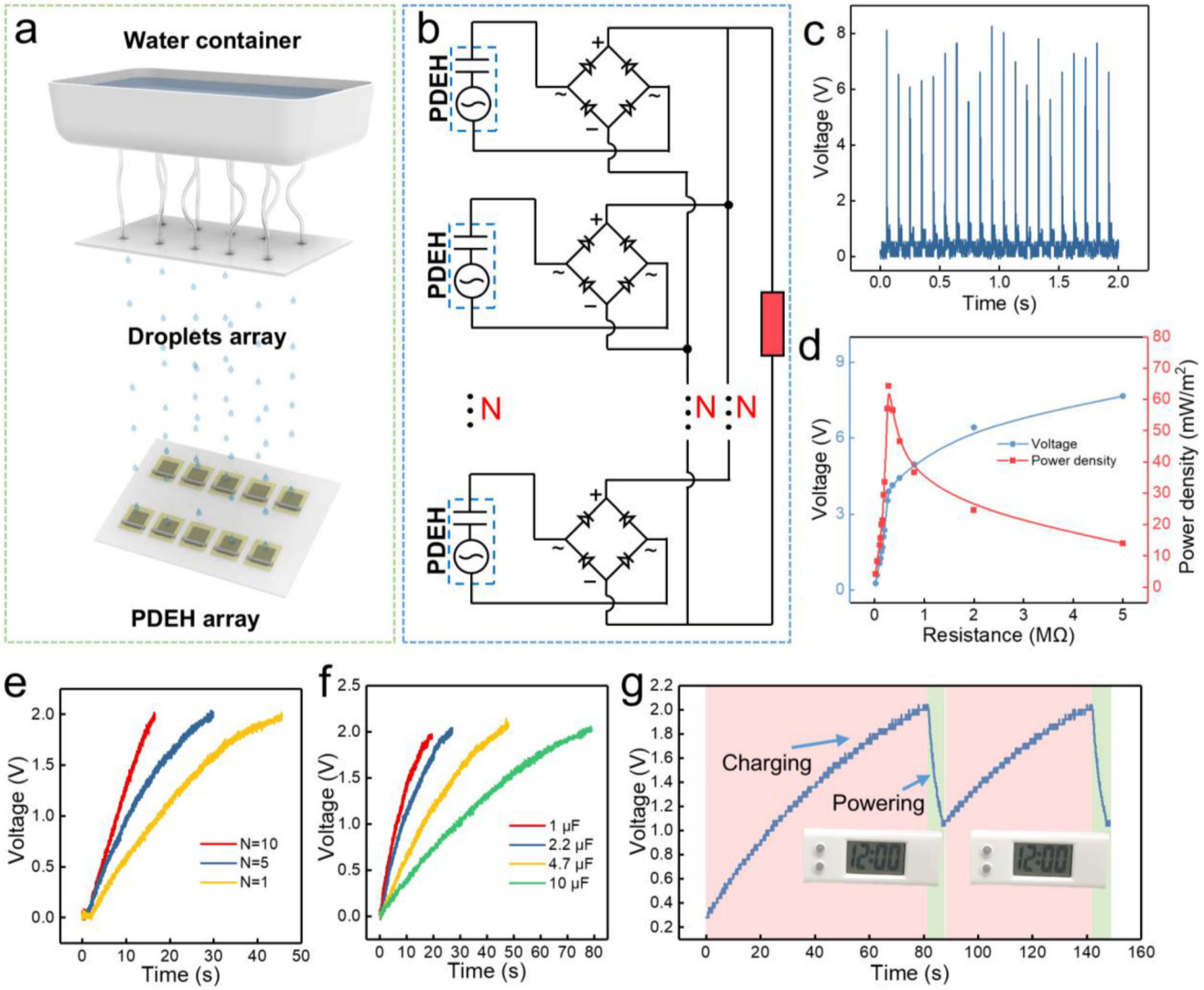


FIGURE 4 | Scalable application and energy-storage demonstration of the pollen-derived droplet energy harvester (PDEH). (a) Schematic illustration of the experimental setup used to simulate rainfall-driven electricity generation using a PDEH array. (b) Equivalent circuit model of a PDEH array consisting of N parallel-connected devices for enhanced charge output. (c) Rectified output voltage of a single PDEH triggered by rainwater droplets. (d) Output power density of a single PDEH under varying external loads, showing a maximum instantaneous power density of 63 mW m^{-2}. (e) Charging curves of a 1 μF capacitor using PDEH arrays composed of different numbers of units (N = 1, 5, and 10), demonstrating scalable charge accumulation. (f) Charging performance of capacitors with different capacitances (1, 2.2, 4.7, and 10 μF) using a 10-unit PDEH array. (g) Demonstration of powering a commercial electronic clock by charging a 10 μF capacitor to 2 V, illustrating closed-loop energy harvesting and storage capability.

the PDEH array was able to charge a 10 μF capacitor to 2 V within 57 s.

3 | Conclusion

In this work, we have demonstrated a pollen-derived droplet energy harvester (PDEH) that converts the mechanical energy of raindrops into electricity using pollen-derived paper from an abundant and renewable biological feedstock as the structural platform. A relatively simple chemical processing workflow converts sunflower pollen into free-standing paper, followed by FDTS fluorination and PANI polymerization to produce the functional layers. The two modified layers are then hot-pressed together, producing an ultrathin (~70 μm), ultralight (0.191 g) multilayer PDEH. The PDEH contains only ~24 wt.% non-renewable solid materials in the final device, while the direct material cost of the incorporated constituents is estimated to be ~US$0.003 per 3 × 3 cm^2 unit. This material cost does not include the additional process consumables used during pollen treatment and functionalization, which are associated with the current laboratory-scale fabrication procedure. The device delivers a practical output of 16.8 V and an energy-conversion efficiency of 1.26% from a single tap-water droplet, achieves a peak power density of 63 mW m^{-2}, and operates reliably on curved or irregular surfaces. The device exhibits no detectable fluorine leaching after 10 000 wetting cycles, and its output remains stable over 14 days, demonstrating excellent durability and environmental safety. A 10-unit PDEH array demonstrates closed-loop functionality by charging a 10 μF capacitor to 2 V within ~80 s and powering a commercial clock under simulated rainfall.

16163028, 0, Downloaded from https://advanced.onlinelibrary.wiley.com/doi/10.1002/adfm.79211 by Nam-Joon Cho - Shanghai Jiaotong University , Wiley Online Library on [21/10/2026]. See the Terms and Conditions (https://onlinelibrary.wiley.com/terms-and-conditions) on Wiley Online Library for rules of use; OA articles are governed by the applicable Creative Commons License

These findings establish pollen-derived films as a compelling and sustainable materials platform for distributed, low-carbon rain-energy harvesting. However, further efforts should be devoted to enhancing the output performance of the PDEH through material optimization and system integration. Overall, the PDEH is expected to inspire new directions in green energy harvesting and the development of self-sustaining electronic systems.

4 | Experimental Section

4.1 | Materials

Raw bee pollen was purchased from Changge Xingchuang Bee Industry Co., Ltd., China. Aniline and Perfluorodecyltrichlorosilane were purchased from Shanghai Aladdin Biochemical Technology Co., Ltd. KOH, acetone, diethyl ether, and HCl were all purchased from Sigma-Aldrich.

4.2 | Defatting of Bee Pollen

To remove the pollen kitt, natural or bee-derived pollen grains were sequentially defatted using water, acetone, and diethyl ether.

Initially, 500 g of bee pollen was dispersed in 1 L of deionized water at 50°C and stirred at 1000 rpm for 2 h using a disperser (IKA). The resulting suspension was filtered through a 200 μm nylon mesh to eliminate large debris and impurities, and the filtrate was subsequently vacuum-filtered to remove excess water. The recovered pollen was then refluxed in 1 L of acetone under continuous stirring (1000 rpm) at room temperature for 3 h. After that, acetone was removed by vacuum filtration, and the sample was repeatedly rinsed (2–3 times) with fresh acetone until the filtrate became clear. The cleaned pollen was transferred onto a glass Petri dish and air-dried in a fume hood for 12 h.

Following acetone treatment, approximately 150 g of dried pollen was redispersed in 1 L of diethyl ether and stirred at 25°C and 1000 rpm for 2 h, and the solvent was removed by vacuum filtration. This step was repeated once using fresh solvent. The pollen was then washed twice with diethyl ether and dispersed again in a new 1 L batch, followed by overnight stirring (12 h) under the same conditions. Finally, the solvent was removed by vacuum filtration, and the fully defatted pollen was air-dried in a fume hood for another 12 h to obtain the purified sample.

4.3 | Fabrication of Pollen Microgel and Original Pollen Paper

5 g of defatted pollen was combined with 50 mL of 10 wt.% KOH solution in a PTFE round-bottom flask. The mixture was stirred at 800 rpm and refluxed at 80°C for 2 h, maintaining a pollen-to-solution ratio of about 1:10 (w/w). The reaction mixture was then filtered through a nylon mesh (pore size: 35–30 μm) using a custom filtration setup, and the filtrate was repeatedly replaced with fresh KOH solution until it appeared completely clear. The pollen residue collected on the mesh was reserved for further processing.

A new batch of 50 mL KOH solution was subsequently added to the filtered pollen, and the suspension was divided equally into two tubes (25 mL each). These tubes were heated at 80°C for 40 h in an oven to complete the de-esterification process. After treatment, the mixture was once again filtered through nylon mesh of identical pore size and washed thoroughly with deionized water until the filtrate pH stabilized at ∼7.5, as verified with pH indicator strips, to get the pollen microgel. Finally, the pollen microgel was poured into a Petri dish and allowed to dry naturally through water evaporation, yielding the pristine pollen paper.

4.4 | Fabrication of PDEH

The fabrication process of the PDEH can be divided into three main steps:

i. Preparation of the conductive pollen paper: A solution was prepared by adding 833 μL of HCl and 2.328 mL of aniline to 50 mL of deionized (DI) water, followed by stirring under an ice bath at 800 rpm for 6 h. The pristine pollen paper was then immersed in this solution. Separately, 3.8 g of ammonium persulfate (APS) was dissolved in 10 mL of DI water, and the resulting solution was added dropwise into the aniline–HCl mixture while maintaining a stirring speed of 50 rpm under ice-bath conditions. The reaction was allowed to proceed for 24 h, after which the pollen paper was removed and washed thoroughly with DI water, yielding the conductive pollen paper.

ii. Preparation of the dielectric pollen paper: A 1 wt.% perfluorodecyltrichlorosilane (FDTS) solution was prepared by dissolving 0.5 g of FDTS in 49.5 g of absolute ethanol. The pristine pollen paper was immersed in this solution for 12 h (overnight), then removed and air-dried, producing the fluorinated dielectric pollen paper.

iii. Assembly of the PDEH: The dielectric pollen paper was sandwiched between a conductive pollen paper (bottom electrode) and a narrow conductive pollen-paper strip (top electrode), and the three layers were laminated by hot pressing (LP-S-20, Labtech Engineering Co., Ltd.) under an applied compressive force of 100 N at 60°C for 10 min.

4.5 | Characterization and Measurements

The electrical output of the PDEH was measured with an oscilloscope (TBS2104B, Tektronix). Time-resolved voltage waveforms were recorded at a sampling interval of 0.4 ms (sampling rate 2.5 kS s^{-1}), which is sufficient to resolve the rising and decaying edges of the droplet-induced voltage pulse. Unless otherwise stated, output voltages are reported as mean ± SD of n = 10 repeated droplet impacts on the same PDEH device for each experimental condition. The error bars therefore reflect measurement-to-measurement variation rather than device-to-device variation. The contact angle was measured using a contact angle meter (Attension Theta Flex C201, Biolin Scientific). The FTIR spectra were obtained using a PerkinElmer Frontier. SEM images were taken using a JEOL JSM-7600F Schottky field-emission scanning electron microscope. XPS measurements were

16163028, 0, Downloaded from https://advanced.onlinelibrary.wiley.com/doi/10.1002/adfm.79211 by Nam-Joon Cho - Shanghai Jiaotong University , Wiley Online Library on [21/10/2026]. See the Terms and Conditions (https://onlinelibrary.wiley.com/terms-and-conditions) on Wiley Online Library for rules of use; OA articles are governed by the applicable Creative Commons License

recorded on an XPS Kratos AXIS Supra. The conductivity of the conductive pollen paper was measured by a multimeter D03124, DURATOOL.

Author Contributions

Zi Hao Guo: conceptualization, methodology, data curation, supervision, formal analysis, validation, investigation, visualization, writing – review and editing, writing – original draft. **Chenchen Zhou**: investigation, validation, methodology, formal analysis, supervision, software, resources. **Hailu Wang**: conceptualization, methodology, formal analysis, investigation. **Jian Li**: investigation, validation. **Jingyu Deng**: investigation, validation. **Yabo Huang**: investigation, validation. **Xiong Pu**: writing – review and editing, conceptualization. **Munho Kim**: supervision, writing – review and editing, resources, funding acquisition, project administration. **Namjoon Cho**: funding acquisition, writing – review and editing, supervision, resources, project administration.

Acknowledgements

This study was supported by the grants from the Ministry of Education in Singapore under grant MOE-MOET32022-0002.

Conflicts of Interest

The authors declare no conflicts of interest.

Data Availability Statement

The data that support the findings of this study are available on request from the corresponding author. The data are not publicly available due to privacy or ethical restrictions.

References

1. U.S. Energy Information Administration, International Energy Statistics: International Electricity Consumption, Electricity Net Consumption, World, Annual Data, https://www.eia.gov/international/data/world.

2. International Energy Agency *Electricity Grids and Secure Energy Transitions IEA Reports* (International Energy Agency, 2023).

3. B. Zhu, Z. Deng, X. Song, et al., "CarbonMonitor-Power Near-Real-Time Monitoring of Global Power Generation on Hourly to Daily Scales," *Scientific Data* 10 (2023): 217, https://doi.org/10.1038/s41597-023-02094-2.

4. D. Navia Simon and L. Diaz Anadon, "Power Price Stability and the Insurance Value of Renewable Technologies," *Nature Energy* 10 (2025): 329–341, https://doi.org/10.1038/s41560-025-01704-0.

5. P. Friedlingstein, M. O'Sullivan, M. W. Jones, et al., "Global Carbon Budget 2025," *Earth System Science Data Discussions* 2025 (2025): 1.

6. C. Campos Morales, E. L. Pakhtigian, J. R. Landry, H. Wiseman, A. T. Pham, and W. Peng, "Designing Retirement Strategies for Coal-Fired Power Plants to Mitigate Air Pollution and Health Impacts," *Environmental Science & Technology* 58 (2024): 15371–15380, https://doi.org/10.1021/acs.est.4c00704.

7. T. Gibon and A. L. Hahn Menacho, "Parametric Life Cycle Assessment of Nuclear Power for Simplified Models," *Environmental Science & Technology* 57 (2023): 14194–14205, https://doi.org/10.1021/acs.est.3c03190.

8. K. Kvashnina, F. Claret, N. Clavier, T. G. Levitskaia, H. Wainwright, and T. Yao, "Long-Term, Sustainable Solutions to Radioactive Waste Management," *Scientific Reports* 14 (2024): 5907, https://doi.org/10.1038/s41598-024-55911-y.

9. J. P. Gwynn, V. Hatje, N. Casacuberta, M. Sarin, and I. Osvath, "The Effect of Climate Change on Sources of Radionuclides to the Marine Environment," *Communications Earth & Environment* 5 (2024): 135, https://doi.org/10.1038/s43247-024-01241-w.

10. P. Rahdan, E. Zeyen, and M. Victoria, "Strategic Deployment of Solar Photovoltaics for Achieving Self-Sufficiency in Europe Throughout the Energy Transition," *Nature Communications* 16 (2025): 6259, https://doi.org/10.1038/s41467-025-61492-9.

11. K. E. Gan, O. Taikan, T. Y. Gan, T. Weis, D. Yamazaki, and H. Schüttrumpf, "Enhancing Renewable Energy Systems, Contributing to Sustainable Development Goals of United Nation and Building Resilience Against Climate Change Impacts," *Energy Technology* 11 (2023): 2300275, https://doi.org/10.1002/ente.202300275.

12. F. J. M. M. Nijsse, J.-F. Mercure, N. Ameli, et al., "The Momentum of the Solar Energy Transition," *Nature Communications* 14 (2023): 6542, https://doi.org/10.1038/s41467-023-41971-7.

13. Ember Energy *Global Electricity Review 2025* (Ember Energy, 2025), https://ember-energy.org/latest-insights/global-electricity-review-2025/.

14. M. Li, R. Shan, A. Abdulla, E. Virguez, and S. Gao, "The Role Of Dispatchability In China's Power System Decarbonization," *Energy & Environmental Science* 17 (2024): 2193–2205, https://doi.org/10.1039/D3EE04293F.

15. I. Riepin, J. D. Jenkins, D. Swezey, and T. Brown, "24/7 Carbon-Free Electricity Matching Accelerates Adoption of Advanced Clean Energy Technologies," *Joule* 9 (2025): 101808, https://doi.org/10.1016/j.joule.2024.101808.

16. J. Guo, H. Wu, T. Ma, et al., "Scenario-Adaptive Hierarchical Optimisation Framework for Design in Hybrid Energy Storage Systems," *Nature Communications* 17 (2026): 657, https://doi.org/10.1038/s41467-025-67377-1.

17. Z. Lin and Z. Yang, "Water Droplet Energy Harvesting," *Droplet* 3 (2024): 97, https://doi.org/10.1002/dro2.97.

18. Meteorological Service Singapore (MSS), *2022 Climate and Weather: The Year in Review* (National Environment Agency, 2023).

19. D. C. Nguyen, M. C. Nguyen, D. T. Pham, et al., "Field Effect Enhanced Electric Double Layer for High-Output Droplet Energy Harvester," *Nano Energy* 134 (2025): 110560, https://doi.org/10.1016/j.nanoen.2024.110560.

20. J. Wang, S. Xu, and C. Hu, "Charge Generation and Enhancement of Key Components of Triboelectric Nanogenerators: A Review," *Advanced Materials* 36 (2024): 41.

21. T. Du, Z. Chen, F. Dong, et al., "Advances in Green Triboelectric Nanogenerators," *Advanced Functional Materials* 34 (2024): 27.

22. J. Meng, L. Zhang, H. Liu, et al., "A New Single-Electrode Generator for Water Droplet Energy Harvesting With A 3 mA Current Output," *Advanced Energy Materials* 14 (2024): 12, https://doi.org/10.1002/aenm.202303298.

23. Y. Qiu, D. Zhang, Z. Zhou, et al., "Hierarchical Assembly of Biomass Fiber-Lamella-Macromolecule Networks for Biocomposites With High Strength and Water-Resistant Sealing," *Proceedings of the National Academy of Sciences of the United States of America* 122 (2025): 12.

24. Y. Hwang, M. Bin Ibrahim, J. Deng, J. Jackman, and N. Cho, "Colloid-Mediated Fabrication of a 3D Pollen Sponge for Oil Remediation Applications," *Advanced Functional Materials* 31 (2021): 8.

25. J. Kim, J. Deng, N. Cho, and S. Han, "Directional, Silanized Plant-Based Sponge for Oil Collection," *Advanced Functional Materials* 34 (2024): 9.

26. F. Li, P. Phyo, J. Jacobowitz, M. Hong, and J. Weng, "The Molecular Structure of Plant Sporopollenin," *Nature Plants* 5 (2019): 41–46, https://doi.org/10.1038/s41477-018-0330-7.

27. Z. Qu and J. Meredith, "The Atypically High Modulus of Pollen Exine," *Journal of the Royal Society Interface* 15 (2018): 20180533, https://doi.org/10.1098/rsif.2018.0533.

28. C. M. Glinkerman, S. Lin, J. Ni, F.-S. Li, X. Zhao, and J.-K. Weng, "Sporopollenin-Inspired Design and Synthesis of Robust Polymeric Materials," *Communications Chemistry* 5 (2022): 9, https://doi.org/10.1038/s42004-022-00729-w.

16163028, 0, Downloaded from https://advanced.onlinelibrary.wiley.com/doi/10.1002/adfm.79211 by Nam-Joon Cho - Shanghai Jiaotong University , Wiley Online Library on [21/10/2026]. See the Terms and Conditions (https://onlinelibrary.wiley.com/terms-and-conditions) on Wiley Online Library for rules of use; OA articles are governed by the applicable Creative Commons License

29. L. Albano, A. Bento, V. Correia, and C. Pereira, "The Chemistry of Sporopollenin Ektexine and Endexine Layers Isolated From Sunflower Pollen Through an Ionic Liquid-Mediated Process," *Acs Omega* 10 (2024): 411–421, https://doi.org/10.1021/acsomega.4c06524.

30. T.-F. Fan, S. Park, Q. Shi, et al., "Transformation of Hard Pollen Into Soft Matter," *Nature Communications* 11 (2020): 10, https://doi.org/10.1038/s41467-020-15294-w.

31. Z. Zhao, J. Deng, H. Tae, et al., "Recyclable and Reusable Natural Plant-Based Paper for Repeated Digital Printing and Unprinting," *Advanced Materials* 34 (2022): 10.

32. T. Guan, S. Yuket, H. Cong, D. W. Carton, and N. Zhang, "Permanent Hydrophobic Surface Treatment Combined With Solvent Vapor-Assisted Thermal Bonding for Mass Production of Cyclic Olefin Copolymer Microfluidic Chips," *ACS Omega* 7 (2022): 20104–20117, https://doi.org/10.1021/acsomega.2c01948.

33. S. Nie, Q. Fu, X. Lin, C. Zhang, Y. Lu, and S. Wang, "Enhanced Performance of a Cellulose Nanofibrils-Based Triboelectric Nanogenerator by Tuning the Surface Polarizability and Hydrophobicity," *Chemical Engineering Journal* 404 (2021): 126512, https://doi.org/10.1016/j.cej.2020.126512.

34. Z. Zhao, Y. Hwang, Y. Yang, et al., "Actuation and Locomotion Driven by Moisture in Paper Made With Natural Pollen," *Proceedings of the National Academy of Sciences* 117 (2020): 8711–8718, https://doi.org/10.1073/pnas.1922560117.

35. Z. Yuan and L. Guo, "Recent Advances In Solid–Liquid Triboelectric Nanogenerator Technologies, Affecting Factors, And Applications," *Scientific Reports* 14 (2024): 10456, https://doi.org/10.1038/s41598-024-60823-y.

36. G. Liu, C. Ji, J. Li, and X. Pan, "Facile Preparation and Properties of Superhydrophobic Nanocellulose Membrane," *Arabian Journal of Chemistry* 15 (2022): 103964, https://doi.org/10.1016/j.arabjc.2022.103964.

37. U. Zulfiqar, N. Kostoglou, A. G. Thomas, C. Rebholz, A. Matthews, and D. J. Lewis, "Flexible Nanoporous Activated Carbon for Adsorption of Organics From Industrial Effluents," *Nanoscale* 13 (2021): 15311–15323, https://doi.org/10.1039/D1NR03242A.

38. M. Trchová, I. Šeděnková, E. Tobolková, and J. Stejskal, "FTIR Spectroscopic and Conductivity Study of the Thermal Degradation of Polyaniline Films," *Polymer Degradation and Stability* 86 (2004): 179–185, https://doi.org/10.1016/j.polymdegradstab.2004.04.011.

39. W. Shao, R. Jamal, F. Xu, A. Ubul, and T. Abdiryim, "The Effect of a Small Amount of Water on the Structure and Electrochemical Properties of Solid-State Synthesized Polyaniline," *Materials* 5 (2012): 1811–1825, https://doi.org/10.3390/ma5101811.

40. N. Zhang, H. Zhang, W. Xu, et al., "A droplet-based electricity generator With ultrahigh instantaneous output and short charging time," *Droplet* 1 (2022): 56–64, https://doi.org/10.1002/dro2.10.

41. H. L. Wang, B. Zhang, T. Chen, W. Mao, and Y. Wang, "High-Efficiency Single-Droplet Energy Harvester for Self-Sustainable Environmental Intelligent Networks," *Advanced Energy Materials* 13 (2023): 2302858, https://doi.org/10.1002/aenm.202302858.

42. S. Niu, S. Wang, L. Lin, et al., "Theoretical Study of Contact-Mode Triboelectric Nanogenerators as an Effective Power Source," *Energy & Environmental Science* 6 (2013): 3576, https://doi.org/10.1039/c3ee42571a.

43. Y. Lee, S. Lakshmi, and J. Ong, "Rain Drop Size Distribution Modelling in Singapore – Critical Diameters," in *The Second European Conference on Antennas and Propagation, EuCAP 2007*, Edinburgh, UK November 11–16, 2007, https://doi.org/10.1049/ic.2007.1028.

Supporting Information

Additional supporting information can be found online in the Supporting Information section.

Supporting File 1: adfm79211-sup-0001-SuppMat.docx.
Supporting File 2: adfm79211-sup-0002-MovieS1.mp4.

16163028, 0, Downloaded from https://advanced.onlinelibrary.wiley.com/doi/10.1002/adfm.79211 by Nam-Joon Cho - Shanghai Jiaotong University , Wiley Online Library on [21/10/2026]. See the Terms and Conditions (https://onlinelibrary.wiley.com/terms-and-conditions) on Wiley Online Library for rules of use; OA articles are governed by the applicable Creative Commons License